International Journal of Biological Macromolecules 268 (2024) 131703

Contents lists available at ScienceDirect

International Journal of Biological Macromolecules

journal homepage: www.elsevier.com/locate/ijbiomac

Insights into the interaction and inhibitory action of palmatine on lysozyme fibrillogenesis: Spectroscopic and computational studies

Arindam Das, Gouranga Jana, Shukdeb Sing, Anirban Basu *

Department of Chemistry and Chemical Technology, Vidyasagar University, Midnapore 721 102, India

ARTICLE INFO

Keywords:
Palmatine
Lysozyme
Fibrillation

ABSTRACT

Interaction under amyloidogenic condition between naturally occurring protoberberine alkaloid palmatine and hen egg white lysozyme was executed by adopting spectrofluorometric and theoretical molecular docking and dynamic simulation analysis. In spetrofluorometric method, different types of experiments were performed to explore the overall mode and mechanism of interaction. Intrinsic fluorescence quenching of lysozyme (Trp residues) by palmatine showed effective binding interaction and also yielded different binding parameters like binding constant, quenching constant and number of binding sites. Synchronous fluorescence quenching and 3D fluorescence map revealed that palmatine was able to change the microenvironment of the interacting site. Fluorescence life time measurements strongly suggested that this interaction was basically static in nature. Molecular docking result matched with fluorimetric experimental data. Efficient drug like interaction of palmatine with lysozyme at low pH and high salt concentration prompted us to analyze its antifibrillation potential. Different assays and microscopic techniques were employed for detailed analysis of lysozyme amyloidosis.Thioflavin T(ThT) assay, Congo Red (CR) assay, 8-anilino-1-naphthalenesulfonic acid (ANS) assay, Nile Red (NR) assay, anisotropy and intrinsic fluorescence measurements confirmed that palmatine successfully retarded and reduced lysozyme fibrillation. Dynamic light scattering (DLS) and atomic force microscopy (AFM) further reiterated the excellent antiamyloidogenic potency of palmatine.

1. Introduction

Various proteins and peptides have ability to self-aggregate by disturbing their original tertiary functional structure under appropriate physiological conditions [1–4]. These types of aggregation lead to formation of highly ordered, rigid and β-sheet enriched amyloid fibrils [5,6]. Deposition of fibrillar aggregates in different parts of our body are closely associated with a wide number of disorders including Alzheimer's, Parkinson's, Huntington's, familial amyloidosis and type-II diabetes [7–13].

Lysozyme, protective enzyme, have been identified in different types of plant, animal and microbes. There are conventionally three types of lysozyme i.e. i. Chicken/Hen type (also known as conventional type or c type) ii. Goose type (g type) iii. Invertebrate's type (i type). Some plant and microbial types have been also separated. Lysozyme can easily rapture bacterial cell wall by hydrolysing glycosidic linkage of peptidoglycan. For this reason it is endowed with natural antimicrobial action against different fungal, bacterial and viral pathogens [14].This enzyme is widely distributed in variety of body fluids and tissues in gastrointestinal tract, kidneys, liver, lymph nodes, spleen, skin, lachrymal and salivary glands [15]. As it has several enzymatic roles to play, its amyloidosis can lead to multi-organ disorders, haemorrhagic complications and different slow-moving life threatening diseases. As mentioned previously neurodegenerative disorders may also lead to autosomal dominant genetic diseases [8,9,16–18].

Lysozyme fibrillation process is a well-studied regular kinetic process [19–24]. Formation of cross β sheet stable structure from α helical shape during fibrillation is monitored through different analytical approaches [5,19,25]. Lysozyme is popularly used as a model system for analysis of protein aggregation [25].

Human lysozyme has 130 amino acid residues with 59 % sequential homology to hen egg white lysozyme (HEWL). HEWL has stable tertiary structure with 129 amino acid residues having α helical, β sheet, loops & turns and some unordered structure composition under different conditions [26–28]. There are two types of natural inherent fluorescence active residues i.e. Tryptophan (Trp) and Tyrosine (Tyr) [28,29]. The active drug binding site of lysozyme is situated at its big hydrophobic crevice which is linked with α helix conformation [30–33]. Lysozyme

* Corresponding author at: Department of Chemistry and Chemical Technology, Vidyasagar University, Midnapore 721 102, India.
E-mail address: anirbanbasu@mail.vidyasagar.ac.in (A. Basu).

https://doi.org/10.1016/j.ijbiomac.2024.131703
Received 29 January 2024; Received in revised form 2 April 2024; Accepted 18 April 2024
Available online 21 April 2024

fibrils are more compatible with fibrillar β-rich structure and it can be stabilized by addition of salt, pH changes or any denaturants [34,35].

Different in-vitro and in-vivo studies have shown that several natural products and synthetic molecules including polyphenols, alkaloids, nanoparticles, dyes, ionic liquids etc. have therapeutic efficiency to inhibit fibrillation of lysozyme [36–51]. Dozens of compounds having these types of antiamyloidogenic capability fail at different stages of clinical trials [52]. So searching for an efficient antifibrillar therapeutic is an important area of current research to fight against the neurodegenerative diseases.

Natural alkaloids are considered to be of potential anti-amyloidogenic value with minimum cytotoxic effect [52].These types of alkaloids have well defined pharmacokinetics and pharmacodynamics with proteins and enzymes [53–57]. Some alkaloids like berberine, palmatine, coralyne, chelerythrine, sanguinarine etc. have conventional drug like static binding in physiological condition with estimated binding free energy ranging from -7 to -5.5 kcal/mol [31,54–57]. Wide range of molecular interactions was reported for the binding of alkaloids with lysozyme. Coralyne actively uses hydrophobic interaction for binding to lysozyme whereas sanguianrine interacts primarily through both hydrogen bonding and hydrophobic interaction [40,56].The binding of the iminium form of chelerythrine with lysozyme is a ground state endothermic process characterized by hydrophobic interactions whereas the binding of alkanolamine form of chelerythrine to lysozyme is an exothermic process primarily driven by hydrogen bonding [31]. Several alkaloids like coralyne, sanguinarine, quinolidine derivative etc. can markedly retard lysozyme fibrillation process with their unique binding capacity primarily through H-bonding and hydrophobic interactions [40,56,58].

Palmatine (Fig. 1) is naturally available protoberberine isoquinoline alkaloid that is generally used as folk medicine in China [59]. It is found in several plants including Chinese gold thread, Gurjo or heart-leaved moonseed, Amur cork tree etc. Many scientific reports suggested that palmatine has pharmacological effects like antioxidation, antiviral, antibacterial, antiinflammatory, neuroprotection, anticancer and regulator of blood lipid control [60–66]. In light of its myriad pharmacological effects we chose this medicinally important alkaloid palmatine as a potential candidate for combating the protein aggregation related ailments. Hen egg white lysozyme and human lysozyme display high scale homologous behaviour including their misfolding and unfolding property which leads to different disorders as mentioned earlier [67]. So in this work we have used hen egg white lysozyme to analyze the anti-amyloidogenic behaviour of palmatine for the first time in the quest for designing therapeutics for protein aggregation related ailments.

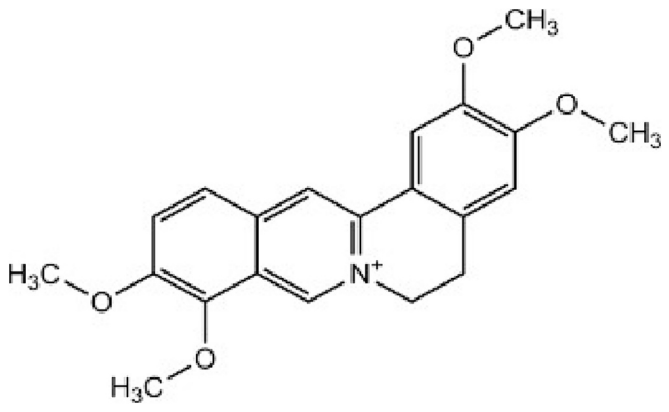

Fig. 1. Molecular structure of palmatine.

2. Experimental

2.1. Materials and stock solutions

Palmatine chloride (PAL)[CAS Number: 10605-02-4], hen egg white lysozyme (HEWL) [CAS Number: 12650-88-3], Thioflavin T (ThT)[CAS Number: 2390-54-7], 8-anilino-1-naphthalenesulfonic acid (ANS), Nile Red (NR)[CAS Number: 7385-67-3], Congo Red (CR)[CAS Number: 573-58-0] along with the buffer components like glycine, sodium chloride and sodium azide were procured from Sigma-Aldrich Corporation (Missouri, USA). All the chemicals were of analytical grade or better. HEWL stock solution was prepared by dissolving it in Glycine-HCl buffer (pH = 2.24; [NaCl] =100 mM; [NaN_3] =1.54 mM). PAL concentration was evaluated by UV-spectrophotometer in double distilled water (ε = 22,500 M^{-1} cm^{-1} at 345 nm) [57].

2.2. Interaction study between HEWL and PAL

2.2.1. Spectrofluorimertic studies

Quenching of emission fluorescence intensity of HEWL by PAL was performed under amyloidogenic condition (pH = 2.24; [NaCl] =100 mM) [40,42] using Hitachi F-7000 spectrofluorimeter, Japan, equipped with Xenon lamp as light source at 293, 298 and 303 K. HEWL (12 μM) was excited at 295 nm and fluorescence emission intensity was recorded over 305–450 nm range with 5 nm excitation and emission slit width in 10 mm quartz cell after successive additions of PAL. All the fluorescence data were corrected for inner filter effect using the following equation [68].

$$F_{corr} = F_{obs} \times e^{\frac{(A_{exi}+A_{emi})}{2}}$$

Quenching data were analyzed after inner filter effect [68] correction by the following Stern-Volmer equation [56].

$$\frac{F_0}{F} = 1 + k_q \tau_0 [Q] = 1 + K_{SV}[Q]$$

where F_0 = fluorescence intensity of HEWL in absence of PAL, F = fluorescence intensity of HEWL in presence of PAL, K_{SV} = Stern-Volmer quenching constant, k_q = quenching rate constant, and [Q] = concentration of PAL.

Then binding constant (K_A) and the number of available binding sites per HEWL (n) was determined using the following equation based on fluorescence titration data [55].

$$log\left(\frac{F_0\text{-}F}{F}\right) = log K_A + n log[PAL]$$

Other thermodynamic parameters like enthalpy (ΔH), entropy (ΔS) and were estimated from Van't Hoff equation:

$$log K_A = -\frac{\Delta H}{2.303RT} + \frac{\Delta S}{2.303R}$$

where R is the universal gas constant and T is the temperature in kelvin. Gibbs free energy (ΔG) was determined from the equation

$$\Delta G = \Delta H - T\Delta S$$

2.2.2. Synchronous fluorescence study

Synchronous fluorescence is generally used to reveal the conformational changes of fluorophores when it binds with the quencher. Here synchronous fluorescence studies were done at Δλ = 15 nm for Tyr residue and Δλ = 60 nm for Trp residue of HEWL [69].

2.2.3. 3D fluorescence study

In recent times 3D fluorescence studies have become popular method for the analysis of conformational changes of protein when it binds with ligand. Comparative analysis of the excitation emission fluorescence

matrix was done using 3D mode of spectrofluorimeter. Both contour diagram and bird's eye view were plotted for native HEWL and HEWL–PAL complex.

2.2.4. Lifetime measurement study

Fluorescence lifetime study is most effective experiment to analyze the decay profile of fluorophores and interpret the binding nature (static or dynamic) between fluorophores and its quencher [70]. The fluorescence lifetime data was recorded on a Horiba J.Y. Fluoro Max (Japan) spectrofluorimeter using the Time Correlated Single Photon Counting (TCSPC) technique. For life time measurement HEWL and its complex with PAL were excited at 288 nm and the emission wavelength was fixed at 338 nm.

Life time was measured by Horiba EZ time software using the following equation [71].

$$F(t) = \sum_{i=1}^{n} \alpha_i exp\left(-\frac{t}{\tau_i}\right)$$

where *F(t)* was fluorescence intensity at time t and α_i was pre-exponential factor at i^{th} time constant. For multi-exponential analysis τ_{avg} was given by [72].

$$\tau_{avg} = \sum \alpha_i \tau_i$$

where τ_i was fluorescence lifetime and α_i was relative amplitude.

2.2.5. ADME-toxicity prediction

Absorption, distribution, metabolism & excretion (ADME) and mutagenicity, tumorigenicity, irritation and reproduction (toxicity) of PAL was forecasted by using Swiss ADME (https://www.swisssimilarity.ch) and OSIRIS property (https://www.organic-chemistry.org).

2.2.6. Docking study

In-silico investigation i.e. molecular docking was performed to analyze the molecular forces involved in the binding between HEWL and PAL [73]. First we prepared the HEWL X-ray crystallographic structure as macromolecular receptor from PDB ID (Protein Data Bank; RSCB) 2ydg [74]. Protein structure was optimized by eliminating crystallographic water & co-crystal ligand (if any). Then polar H and appropriate Kollman charges were spread over the whole receptor macromolecule. 3D structure of PAL as a ligand were retrieved using compound CID 19009 from Pub Chem. Ligand geometry were also optimized by minimizing energy (with ultrasoft pseudopotential) (Fig. S1) and applying Gasteiger charges. At final step of docking command line based open source software AutoDock 4.2.6 (Scripps Research Institute) was used. Docking site of protein structure was characterized by big hydrophobic cavity and the amino acid residues of HEWL [75]. All 50 runs were done over 300 population size and 2,500,000 energy evaluations using RMSD tolerance 2 Å by Genetic Algorithm [76]. All HEWL residues were taken as rigid part to get better docking score [77]. Result visualization and analysis were finalized with help of Discovery Studio Visualizer and Get Area Web server.

2.2.7. Molecular dynamics (MD) simulation

MD simulations were employed to analyze the time dependent in silico investigation of HEWL-PAL interaction. MD simulation was carried out on gromacs-2023.3 software package [78]. Best docking HEWL structure was optimized at pH 2.2 through PROPKA 3.1 (https://www.playmolecule.com). PAL was prepared at SwissParam (http://www.swissparam.ch/) in CHARMM general force field. HEWL was also optimized in same force field. System was solvated in 1 nm dodecahedron box with spc216 (simple point charge) maintaining 100 mM NaCl concentration. Then 100 ns MD run was performed at 298 K temperature using standard protocol.

2.3. Fibril formation and inhibition kinetics

2.3.1. Preparation of HEWL fibrils

40 mg HEWL was dissolved in freshly prepared 2 ml Gly-HCl buffer. Then 1 ml of HEWL solution was taken in a 50 ml conical flask and diluted to 20 ml with buffer. After that the HEWL solution in conical was stirred with tiny stirring magnetic bar (250 rpm) at 55 °C [79,80]. Similar solutions were prepared in other conicals and varying concentrations of PAL (250, 200, 150, 100 and 50 μM) was added and it was also stirred under same condition. Then 800 μl aliquots from each conical was withdrawn at 30 min time intervals for the following experiments. Total incubation time for fibrillation process was 8 h.

2.3.2. ThT assay

Stock solution of ThT was prepared in aqueous medium. The concentration of ThT was determined as reported previously [81]. To monitor the kinetics of HEWL fibrillation in absence and presence of PAL 150 μl of HEWL samples taken at different time intervals during fibrillation process were mixed with 750 μl buffer. After that ThT solution was added to this solution maintaining the final concentration at 25 μM. Final solution was homogenized thoroughly and placed in dark for 1 h. Then the emission fluorescence intensity was recorded at 486 nm by exciting the samples at 440 nm using Hitachi F-7000 spectrofluorometer. This same process was repeated with HEWL fibril developed in presence of different concentrations of PAL.

2.3.3. CR binding assay

CR binding assay is extensively used for the characterization of in vitro amyloid fibrillar growth. A stock solution of CR was prepared and 50 μL aliquots of HWEL solutions in absence and presence of PAL taken at 30 min time interval were strained with CR. The final concentration of CR was adjusted to10 μM in 1 ml of the buffer solution. After that, it was properly homogenized and incubated for 30 mins. The absorption spectrum (400–800 nm) of each sample was recorded on Shimadzu UV-1700 spectrophotometer (Shimadzu Ltd. Japan).

2.3.4. ANS binding assay

ANS stock solution was prepared in double distilled water and concentration was determined spectrophotometrically [82]. 50 μl of each stock solution of fibril was diluted in 750 μl buffer. After that aqueous ANS solution was added to it so that final ANS concentration was 25 μM. Finally emission fluorescence spectra of each sample was recorded by exciting it at 370 nm in the wavelength range 400 to 600 nm.

2.3.5. NR binding assay

A stock solution of 1 mM NR was prepared prior to use [83]. 50 μl of aliquots of the HEWL sample withdrawn for 8 h at 30 min time interval were diluted with 700 μl of buffer solution. Then appropriate volume of NR solution- was added to it so that the final concentration of NR in the mixture was 1 μM. The mixture was stored in dark for 30 min. Thereafter, fluorescence study was performed by exciting the samples at 550 nm.

2.3.6. Intrinsic fluorescence measurements

50 μl of HEWL sample solutions, taken at different time intervals during fibrillation process was diluted to 750 μl with the buffer. Then the intrinsic (Trp) fluorescence intensity of each HEWL sample without and with PAL was recorded at the emission maxima of 338 nm by exciting the samples at 295 nm.

2.3.7. Fluorescence anisotropy measurements

Fluorescence anisotropy was performed by using the aliquots collected at 30 mins time interval during fibril formation. Amyloid samples were diluted to 10 μM by buffer solution. The fluorescence anisotropy value (*r*) was obtained using the following equation

$$r = \frac{I_{vv} + GI_{vh}}{I_{vv} + 2GI_{vh}}$$

where I_{vv} and I_{vh} are the vertical and horizontal components with respect to excitation by vertically polarized light at 280 nm. G is the instrumental correction factor for correcting polarizing effects in the emission monocromator and detector, given by $G = I_{vh}/I_{hh}$ [84].

2.3.8. Dynamic light scattering (DLS) measurements

DLS is powerful technique, generally used to determine the hydrodynamic size of particle. We have used this technique to monitor the growth pattern of HEWL in absence and presence of PAL. Size of HEWL fibrillar species was determined using Malvern Zetasizer Pro, United Kingdom.

2.3.9. FTIR studies

FTIR spectral analysis of different samples during fibrillation process was done using Perkin Elmer spectrophotometer which was equipped with Zinc Selenide (ZnSe) Attenuated Total Reflectance (ATR), KBr beam splitter and $LiTaO_3$ detector (Perkin Elmer, USA).

2.3.10. Circular dichroism (CD)

Circular Dichroism (CD) spectra were recorded for native HEWL, HEWL fibril and HEWL + PAL fibril using Jasco J-1100 CD spectrophotometer (Japan) over the range of 190 to 260 nm. All CD spectra were taken after three fold dilution of the samples with Gly-HCl buffer. CD spectral data were analyzed using "CONTINLL" program of DICHROWEB considering dataset 4 as reference [85–89].

2.3.11. AFM imaging

Direct visualization and morphological study of HEWL fibrils were completed using Agilent 5500 (Santa Clara, California, USA) atomic force microscope equipped with 100 μm silicon cantilever. Cantilever was oscillated at 150 kHz frequency when force constant was 42 N/m. Silicon Nitride tips with 10 nm curvature were used. 200 times diluted fibrillar samples were drop casted over microscopic glass cover slip. Images were analyzed and characterized by Gwyddion 2.6.2 (Czech Metrology Institute).

2.4. Statistical analysis

All data are represented as mean ± standard deviation of four independent determinations.

3. Results and discussion

3.1. Analysis of the interaction between HEWL and PAL

3.1.1. Intrinsic fluorescence quenching studies of HEWL by PAL and different binding parameter determination

Photophysical properties of the protein fluorophores are highly sensitive to micro environmental polarity change so fluorescence can be a useful probe for protein ligand interaction study [90,91]. Hence to find out the mode, mechanism and nature of binding interaction intrinsic fluorescence quenching study of HEWL in presence of PAL is performed. HEWL has two types of fluorescence active residues i.e. Tryptophan (TRP) and Tyrosine (TYR) but when HEWL is excited at 295 nm TRP residue is mainly excited. TRP-28, 108, 111, 123 are present in α domain while 62, 63 and 108 are present in substrate binding site [92].TRP-62 and 63 are more exposed and also highly sensitive to chemical changes in their microenvironment [93]. Therefore addition of PAL in HEWL mostly affect these two residues.

Systematic decrease in fluorescence emission intensity of HEWL with successive addition of PAL is shown in Fig. 2 which indicates strong binding of PAL with HEWL under amyloidogenic condition. Fluorescence quenching is accompanied by a bathochromic shift of 28 nm

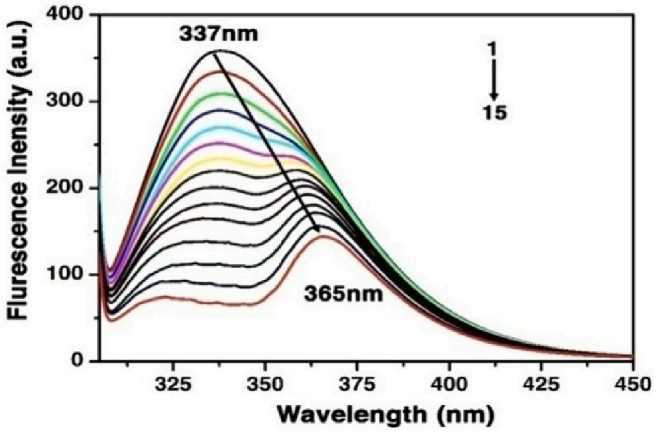

Fig. 2. Intrinsic fluorescence change of HEWL (curve 1, 12 μM) after addition of 2.5, 5, 7.5, 10, 12.5, 15, 17.5, 20, 25, 30, 35, 40, 45 and 50 μM PAL (curves 2 to 15).

indicating that interacting Trp residues have moved towards more hydrophilic region [94,95].

Quenching rate constant (k_q) and Stern-Volmer quenching constant (K_{SV}) for this quenching is (3.74 ± 0.54) × 10^{12} M^{-1} s^{-1} (considering average life time; τ_0 is 10^8 s) and (3.74 ± 0.54) × 10^4 M^{-1}, respectively, at 298 K (Fig. S2).

3.1.2. Synchronous fluorescence studies

Microenvironmental changes of inherent fluorophores like TYR and TRP for HEWL are analyzed through synchronous fluorescence technique [69,96]. In Fig. 3A, when Δλ = 60 nm there was 4 nm (277 nm to 281 nm) red shift of emission maxima. This result signifies that the TRP residues shift closer to hydrophilic environment and becomes more exposed to the solvent system. Although at Δλ = 15 nm a significant synchronous fluorescence quenching is observed but no significant alteration in the emission maxima is noted (Fig. 3B). Overall synchronous fluorescence spectral analysis reveals that TRP residues are more affected than TYR residues during the interaction of PAL with HEWL.

3.1.1. 3D fluorescence study

Quenching visualization and microenvironmental changes of fluorophores are analyzed by using excitation-emission fluorescence 3D matrix [97]. Both contour and bird's eye views of native HEWL and HEWL-PAL complex are shown in Fig. 4. Peak 1 corresponds to the characteristic spectral behaviour of the two protein fluorophores i.e. TRP and TYR present in HEWL [98]. HEWL (6 μM) shows 58 nm and

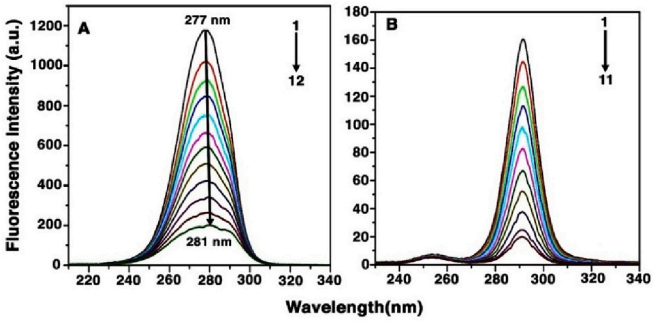

Fig. 3. Synchronous fluorescence spectral changes (excitation) of HEWL on addition of PAL; (A) 10 μM HEWL (curve 1) treated with 2, 4, 6, 8, 10, 12, 14, 16, 18, 22 and 24 μM PAL (curves 2–12) for Δλ = 60 nm (B) 10 μM HEWL (curve 1) treated with 2, 4, 6, 8, 10, 12, 14, 16, 18, and 20 μM PAL (curves 2–11) for Δλ = 15 nm.

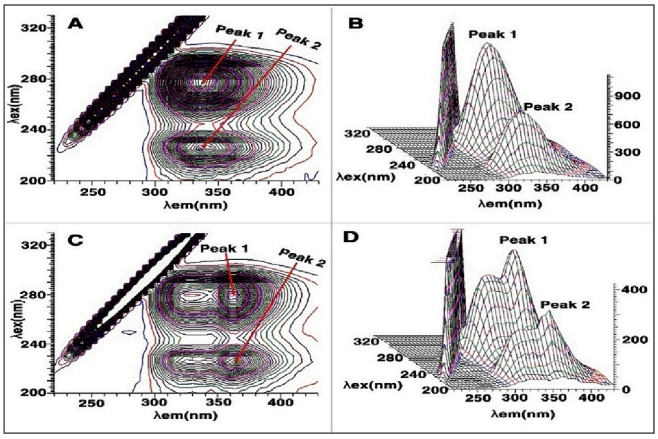

Fig. 4. 3D fluorescence excitation emission matrix of HEWL (A & B) and HEWL + PAL complex (C & D); A & C are contour diagrams and B & D are the bird's eye view.

111 nm Stokes Shift for peak 1 and peak 2 but in presence of PAL Stokes Shift increase up to 85 and 139 nm with significant reduction in fluorescence intensity. This observation is well concurrent with the steady state fluorescence quenching and synchronous fluorescence spectroscopic data. Peak 2 appear due to the characteristic n → π transition of peptide backbone of HEWL. So PAL interaction cause slight unfolding of the polypeptide chain with simultaneous conformational change and exposure of HEWL fluorophores to more polar hydrophilic environment compared to its native state.

3.1.3. Fluorescence life time measurement

Effective distinction between static and dynamic quenching can be established by fluorescence life time measurement [99]. In static quenching mechanism there is no significant alteration in life time but dynamic quenching mechanism is accompanied with an alteration in fluorescence life time. All life time measurements were taken at 338 nm by exciting the samples at 288 nm. From lifetime data it is clear that there is no significant alteration in life time for HEWL and HEWL-PAL complex (Fig. S3). It is difficult to find out finger print decay for each and every Trp residue, especially when macromolecular protein contains multiple TRP residues [100]. So individual lifetime components are not designated instead average lifetime values are reported for qualitative analysis as per standard protocol. The calculated value of average lifetime for native HEWL and its complex with PAL are 0.99 ns and 0.93 ns, respectively. So binding mechanism is static i.e. ground state complex formation takes place during interaction of HEWL with PAL.

3.1.4. Spectrofluoremetric estimation of binding constant and thermodynamic parameters

Apparent binding constant (K_A) is determined to be (3.98 ± 0.19) × 10^4 M^{-1} with a single binding site (n = 1.02 ± 0.05) (Fig. S4) at 298 K from the double log plot [101]. The K_A values are evaluated to be (4.16 ± 0.21) × 10^4 M^{-1} and (3.80 ± 0.18) × 10^4 M^{-1}, respectively, at 293 and 303 K. Enthalpic (ΔH) contribution is –(1.59 ± 0.07) kcal/mol and entropic contribution at 298 K ($T\Delta S$) is (4.68 ± 0.12) kcal/mol for binding of PAL with HEWL. Gibbs free energy change (ΔG) is calculated to be -(6.27 ± 0.19) kcal/mol at 298 K.

3.1.5. ADME-toxicity analysis

In silico ADME-Toxicity prediction is a very important step for drug discovery because this can reportedly predict drug likeness behaviour in our body. Drug score of PAL is 0.692 with zero Lipinski rule violation [102]. PAL also has high gastrointestinal absorption according to BOILED egg approach. Skin permeation (log K_p) and synthetic accessibility of PAL is −5.79 cm/s and 3.18, respectively. Some ADME parameters of PAL are compared with that of the popular anti-amyloidogenic drug Donepezil hydrochloride available in market (Table 1).

From this comparison it is clear that PAL has comparable drug potential with Donepezil hydrochloride. On other hand PAL has indication of nontumorigenic, nonirritant and nonmutagenic properties.

3.1.6. Docking study

Docking results are very similar and support the experimental results (Table 2). All the conformers of HEWL-PAL complex from docking confirm that PAL binds to enzymatic site of HEWL. Gibbs free energy of binding is calculated using following equation [77].

$$\Delta G_{binding} = \Delta G_{vdW} + \Delta G_{elec} + \Delta G_{Hbond} + \Delta G_{desolv} + \Delta G_{tors}$$

For easy interpretation of best conformation of cluster we analyze only the lowest docking conformation, i.e. -5.83 kcal/mol (PDB ID-2ydg) as Gibbs free energy ($\Delta G_{binding}$). The sum of hydrogen bonding energy, van der Waal's energy and desolvation energy is −5.88 kcal/mol and on adding the electrostatic energy (−1.14 kcal/mol) it affords the final intermolecular energy (ΔE_1 = −7.02 kcal/mol). Torsional free energy (ΔE_2) was +1.19 kcal/mol due to eight active torsions between O_1 and C_17, O_1 and C_24, O_2 and C_18, O_2 and C_23, O_3 and C_19, O_3 and C_25, O_4 and C_21, O_4 and C_26 in PAL. The total internal energy (ΔE_3) and unbound system's energy (ΔE_4) are exactly same i.e. -0.43 kcal/mol. All the interacting residues are presented in both 3D and 2D conformation (Figs. 5 & 6). TRP 63 residue makes two conventional H-bonds with PAL whereas GLU 35 has electrostatic pi-anaionic interaction (Fig. S5). ASN46, ASP52, TRP62 build significant interaction through carbon hydrogen bonding whereas TRP63, TRP108, ALA107, ILE98, VAL109, GLU35, ALA110 residues of HEWL are involved in hydrophobic interactions (like alkyl, pi-alkyl, pi-sigma hydrophobic etc.).

Difference in accessible surface area (ASA) of HEWL-PAL complex to native HEWL also justifies sensitive binding between HEWL and PAL.

$$\Delta\text{ASA} = \text{ASA}_{HEWL} - \text{ASA}_{HEWL+PAL}$$

Total ASA of native HEWL and HEWL with PAL is 6538.57 and 6434.63 $Å^2$, respectively. So ASA of native HEWL is reduced because after complexation some ASA of HEWL is seized by the PAL molecules (Fig. S5). ASA of every significant interacting residue (Table 3) which is close to interacting site i.e. big cavity of HEWL, is influenced by these interactions.

3.1.7. MD simulation

MD simulation, very useful modern computational technique, is generally used to analyze the flexibility of macromolecular interaction at experimental conditions. Ligand can change the conformation of macromolecular protein. The stability of protein ligand complex can be revealed by dynamic simulation. Different types of parameters such as root mean square deviation (RMSD), root mean square fluctuation (RMSF), radius of gyration (Rg) etc. are generated to explain the stability and accuracy of structure (Fig. 7). Average RMSD of HEWL in presence and absence of PAL is 0.12 and 0.11 nm, respectively. This RMSD result suggested that HEWL has some deviation and less relative stability in presence of PAL compared to its native form. RMSF of total 129 residues of bound and unbound HEWL are plotted. It shows that HEWL-PAL complex has lower RMSF than unbound HEWL. This implied that some residual flexibility is arrested by PAL. R_g value indicates the structural (tertiary) volume of HEWL. Average R_g value of HEWL and HEWL-PAL complex is 1.39 and 1.38 nm, respectively. Lower R_g value suggests that HEWL has more compact figure when it binds to PAL. Average distance from center of ligand to most important TRP 62, TRP 63 and TRP 108 residues during 100 ns run time are 5.98, 9.78 and 14.14 Å, respectively. H-bond fluctuation is also plotted with 0.35 nm limiting distance.

Table 1
Important ADME parameters of PAL and Donepezil hydrochloride.

Compound	Molecular weight (g/mol)	Lipophilicity (Log P)	Number of hydrogen bond acceptor	Number of rotatable bonds	Total polar surface area (Å^2)	Drug score
PAL	352.40	2.64	4	4	40.80	0.69
Donepezil hydrochloride	379.49	4.00	4	6	38.77	0.63

Table 2
Results of interaction between HEWL (2ydg) and PAL from molecular docking analysis.

Minimum docking energy (kcal/mol)	−5.57
Reference RMSD	53.62
Inhibition constant (K_i) (μm)	82.56
Interacting residues of conventional H bond	TRP63
Conventional hydrogen bonding distance (Å)/ energy (kcal/mol)	1.841/−5.71
Residues involving hydrophobic interaction	ILE98,ALA107,TRP108, VAL109

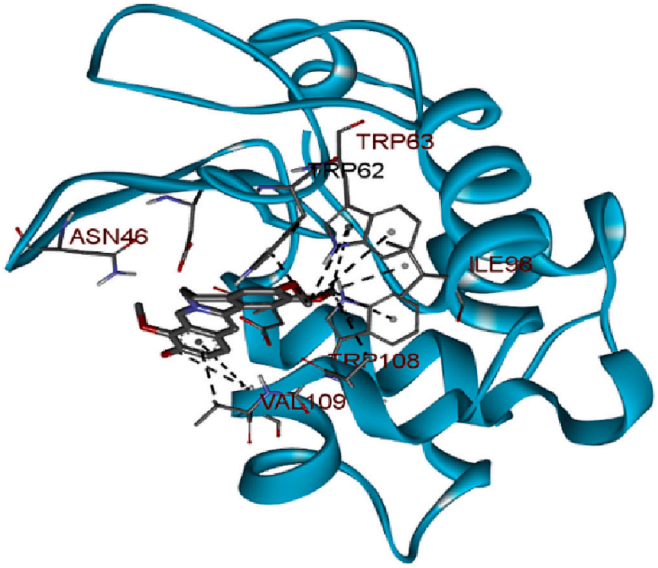

Fig. 5. 3D conformation of PAL interacting with HEWL (2ydg).

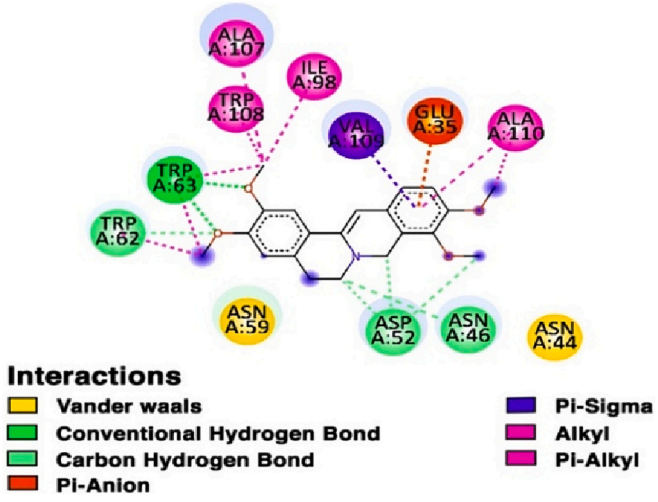

Fig. 6. 2D images displaying all significant interactions between HEWL and PAL.

Table 3
ASA value of HEWL residue and change in ASA during complexation.

Residues	ASA (Å^2) in HWEL only	ASA (Å^2) in HWEL + PAL complex	ΔASA (Å^2)
ASN 46	48.22	27.08	21.14
SER 50	0.77	0.63	0.14
ASP 52	25.06	0.00	25.06
GLN 57	12.69	1.68	11.01
ILE 58	3.27	0.20	3.07
TRP 62	136.11	117.71	18.4
TRP 63	23.50	5.16	18.34
ILE 98	6.84	0.45	6.39
ASP 101	95.91	94.67	1.24
ALA 107	48.73	20.15	28.58
TRP 108	10.87	0.00	10.87
VAL 109	99.63	67.02	32.61
ALA 110	16.29	5.40	10.89

3.2. Fibrillation analysis

3.2.1. ThT assay

Thioflavin T (ThT), a histochemical benzothiazole dye, is regularly used for the investigation of kinetics of formation of fibrillar assemblies of proteins in low pH medium because it can quantitatively stain the stacked β sheet fibrils [103]. Fluorescence emission intensity data of ThT stained HEWL in absence and presence of PAL are noted at different time intervals of fibril growth and plotted against reaction time after inner filter correction. Plots are sigmoidal in nature. These curves show that there is no change in fluorescence intensity till 2.5 h. After that in absence of PAL, a rapid increment in fluorescence intensity is observed till 6 h. In presence of PAL these increment in fluorescence intensity is delayed and reduced markedly. Initially ThT has very low fluorescence emission intensity at 486 nm but upon binding with amyloid fibril its fluorescence enhances rapidly due to molecular rotor nature of ThT. Therefore fluorescence emission intensity is directly proportional to extent of fibril present in solution. So here PAL has strong inhibitory effect over HEWL fibril growth (Fig. 8A). The inhibitory efficiency is calculated using the following equation

$$Inhibitory\ efficiency = \frac{I_0\text{-}I}{I_0} \times 100\%$$

where I_0 and I are fluorescence intensity of ThT in the absence and presence of PAL. After 8 h PAL (250 μM) markedly reduces HEWL amyloid fibrillation by 86.42 % (Fig. 8B).

This comparative kinetic sigmoidal plot with lag, elongation & plateau phases clearly reveal the characteristic pattern of HEWL fibril formation (Fig. 8A). The sigmoidal curves are given by the following Eq. [104].

$$F = A_2 + \frac{(A_1 - A_2)}{1 + e^{-\left\{\frac{(t-t_0)}{\tau}\right\}}}$$

where F, A_2 and (A_1-A_2) denote the fluorescence at time t, initial fluorescence (baseline) and maximum fluorescence intensity, respectively. t and t_0 are the measured time and time required to reach 50 % of maximum fluorescence. Value of aggregation constant (τ) is obtained by nonlinear regression. The lag phase and apparent growth rate constant

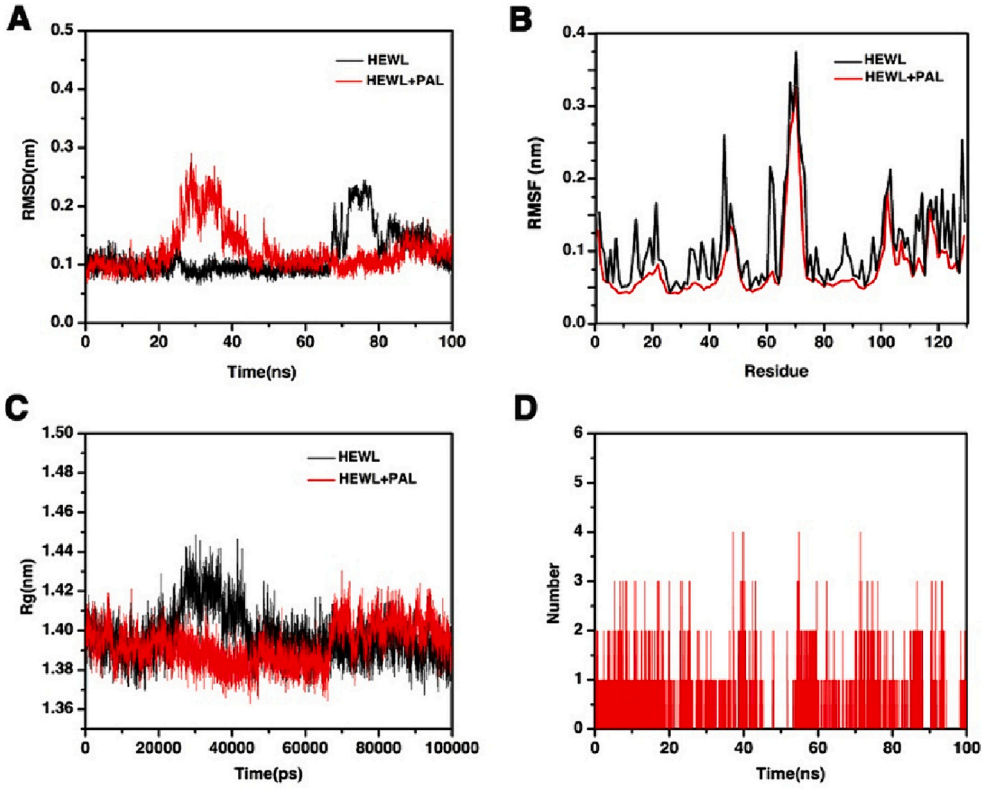

Fig. 7. Molecular dynamics of PAL binding to the HEWL. (A) RMSD plot as a function of time. (B) Backbone residual fluctuations (RMSF) plot. (C) Time evolution of radius of gyration (R_g). (D) The average number of hydrogen bonds between PAL and HEWL residues.

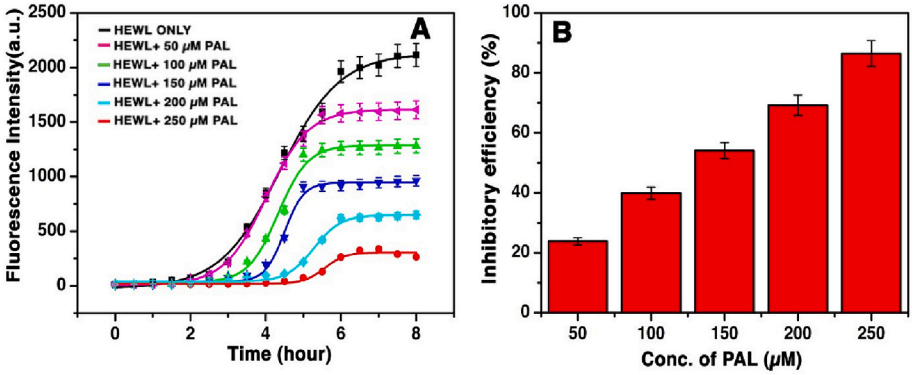

Fig. 8. (A) ThT fluorescence kinetic study of fibrillation of HEWL in prescence of different concentrations of PAL (B) Inhibitory efficiency of PAL on HEWL amyloid fibrillation.

(k_{app}) is given by t_0-2τ and 1/τ, respectively. t_0 and lag phase for only HEWL fibrillation (control) is (4.84 ± 0.17) and (2.79 ± 0.10) hours, respectively, whereas for HEWL-PAL (250 μM) system it is estimated to be (5.56 ± 0.22) and (5.13 ± 0.18) hours, respectively. Significant reduction of fluorescence intensity, delayed elongation period and other kinetic parameters testify that PAL has strong inhibitory influence over HEWL aggregation.

3.2.2. CR assay

CR assay is used to detect fibrillation as a complementary analysis to ThT assay. There are two binding sites of CR in amyloid which are parallel and anti-parallel to β sheet [105,106]. CR exhibits apple green birefringent cross-polarized light on binding with fibrils and this has been used as a qualitative tool for monitoring fibril formation [107]. Comparative absorbance at 543 nm of both sample and control are plotted against time (Fig. S6). Both the curves are sigmoidal in nature having three different phases as seen in ThT study. Outcome of CR study reveals 46 % reduction in absorption intensity of LSZ fibril when it is treated with PAL.

3.2.3. ANS assay

ANS, hydrophobic fluorescent probe, has strong binding affinity towards the hydrophobic region of HEWL. ANS probe displacement study indicates the extent of exposure of hydrophobic sites towards surface. Amyloid HEWL possess higher hydrophobicity than native HEWL because the hydrophobic sites are buried in compact folded structure in native HEWL. In aqueous acidic buffer ANS is weakly fluorescent but fluorescence intensity increases tremendously after binding with amyloid fibrils [108,109]. The increase in fluorescence intensity of ANS with time indicates that hydrophobic patches become more exposed after

amyloid formation which leads to its binding with ANS through hydrophobic interaction. The fluorescence intensity of HEWL treated with ANS is 88 % diminished in presence of 250 μM PAL which indicates that PAL can prevent the movement of hydrophobic part of HEWL towards surface (Fig. 9A). Relatively less blue shift (16 nm) of fluorescence emission maxima of HEWL-PAL system also testifies for the intactness of HEWL tertiary structure.

3.2.4. NR assay

NR is a non-ionic fluorescent dye widely used to study environmental changes specially related to hydrophobicity in biomacromolecules. During the formation of fibrillar aggregates tertiary structure of HEWL changes and a simultaneous change in surface hydrophobicity also takes place. The fluorescence intensity of NR is sensitive to surface hydrophobicity and tertiary structural change in HEWL [110]. The pattern of increase of fluorescence of NR was quite similar to the pattern of ThT fluorescence evolution.

Initially there is no change in fluorescence intensity i.e. lag phase, then there is sudden jump in fluorescence intensity, i.e. growth phase and ultimately fluorescence intensity slightly changed and the curve becomes parallel to time axis, i.e. equilibrium phase. Decrease in fluorescence intensity of HEWL samples treated with PAL indicates that the change in surface hydrophobicity and microenvironment of HEWL under amyloidogenic condition is arrested in presence of PAL (250 μM) (Fig. 9B & Fig. S7). Initially the emission maxima for HEWL sample, i.e. before the fibril formation is at 659 nm which shows a blue shift of 24 nm after fibrillation. In presence of PAL the emission maxima is relatively less blue shifted (only 12 nm). Decrease in the extent of blue shift and fluorescence increase of HEWL samples upon treatment with PAL suggests suppression of tertiary structural changes in HEWL which in turn implies inhibition of amyloid fibrillation.

3.2.5. Intrinsic fluorescence study

Tryptophan is a prominent inherent natural fluorescent amino acid residue generally used to analyze tertiary structural changes of a protein. In HEWL there are six Trp residues (Trp 28, Trp 62, Trp 63, Trp 108, Trp 111 and Trp 123) but among them Trp 62, Trp 63 &Trp 108 are actively present at binding site [29,111]. When we excite the HEWL sample at 295 nm, fluorescence emission at around 338 nm is observed. The change in intrinsic fluorescence intensity at the emission maxima of HEWL samples before and after fibrillation both in the presence and absence of PAL is shown in Fig. 10A. Such drastic alterations in Trp fluorescence emission intensity are the indication of changes in the tertiary structure of HEWL upon fibrillation. Significant decrease in fluorescence quantum yield and red shift (11 nm) of emission maxima of Trp suggest that the Trp residues are exposed from a hydrophobic to a more hydrophilic environment. This decrease can also be for the different quenching mechanisms by the neighbouring amino acid residues of HEWL [112–116].The extent of decrease in intrinsic fluorescence intensity of HEWL samples is relatively less in presence of PAL. HEWL-PAL system shows no prominent shift in emission maxima during fibrillogenesis. These observations indicate that change in the local environment surrounding the Trp residues are arrested in presence of PAL suggesting suppression of amyloid fibrillation of HEWL.

3.2.6. Anisotropy measurement

Anisotropy is a useful probe to study the extent of agitation of a protein residue upon binding to interacting molecules. Anisotropy also provides information about the flexibility of this residue in the macromolecular proteinous environment [70,117]. Here we have studied the steady state Trp fluorescence anisotropy to monitor fibrillation of HEWL both in presence and absence of PAL (Fig. 10B). The anisotropy values of HEWL increase upon fibrillation which indicates that the local environment of Trp residues become more compact with restricted motion. In presence of PAL anisotropy value decreases from 0.15 to 0.09 indicating PAL suppresses the fibrillation of HEWL.

3.2.7. DLS study

Hydrodynamic radii (r_h) of HEWL fibrillar aggregates are determined at different concentration of PAL using dynamic light scattering technique. The mean r_h is estimated using following Stokes - Einstein equation [118].

$$r_h = \frac{kT}{6\Pi\eta D}$$

where k, η and D are Boltzmann's constant, viscosity of medium and diffusion constant at temperature T.

From Table 4 it can be seen that r_h of HEWL fibrils is somewhat larger compared to those in presence of PAL. With increasing concentration of PAL the r_h decreases gradually suggesting breakdown of matured fibril in presence of PAL (Table 4; Fig. S8). At 250 μM concentration of PAL there is significant reduction in fibrillar growth which is also supported by imaging analysis.

3.2.8. FTIR analysis

IR spectra of HEWL and fibril of HEWL after 8 h in the absence and presence of PAL are shown in Fig. 11A. Secondary structure of protein is analyzed by characterizing Amide *I*, Amide II and Amide III bands in the region 1700 to 1200 cm^{-1}. Most important Amide I band spanning from 1600 to 1700 cm^{-1} arise predominantly due to C═O stretching of protein backbone. In Amide I band many assignments can be made like β sheet at 1610–1635 cm^{-1}; random coil at 1630–1645 cm^{-1}; α helix at 1648–1660 cm^{-1}; β turn and anti-parallel β sheet at 1665–1695 cm^{-1} [119,120].

Here native HEWL has a sharp peak at 1649 cm^{-1}s suggesting predominantly α helical conformation. After fibrillation this peak shows a significant blue shift to 1626 cm^{-1}which clearly indicates the formation of β sheet rich fibrillar conformation. In presence of PAL absorption intensity at 1626 cm^{-1} is relatively low compared to HEWL fibril

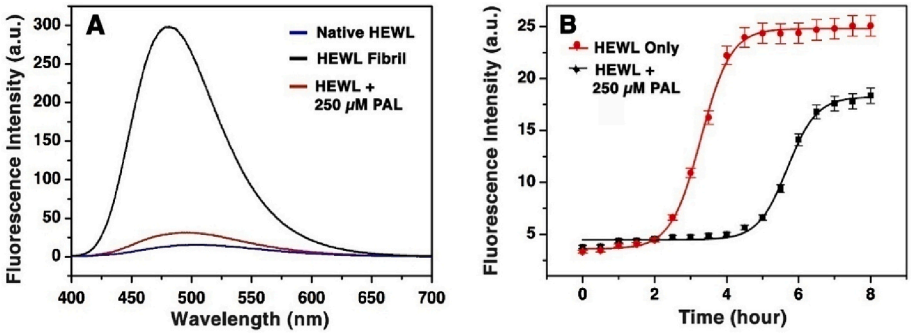

Fig. 9. (A) ANS fluorescence spectral change of HEWL before and after fibrillation both in the absence and presence of PAL and (B) Change in fluorescence intensity of NR at the emission maxima with time for HEWL and HEWL-PAL complex.

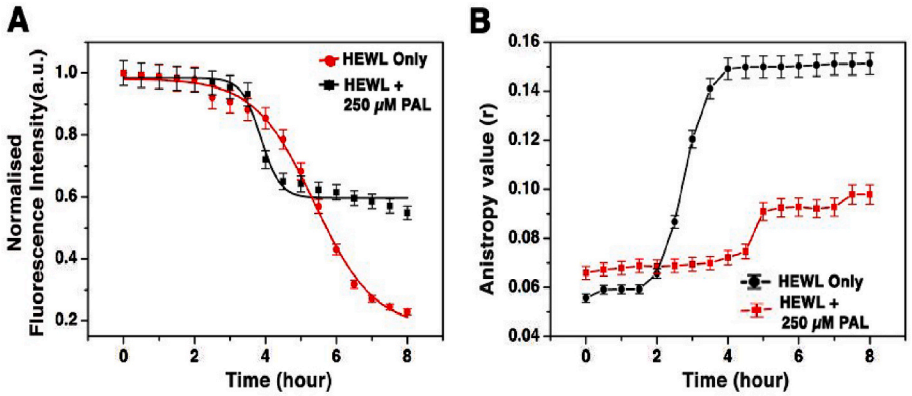

Fig. 10. (A) Change in intrinsic fluorescence with time at emission maxima of HEWL samples in the absence and presence of PAL. (B) Change in anisotropy value of HEWL upon fibrillation in the absence and presence of PAL.

Table 4
Hydrodynamic radius of HEWL fibril and HEWL – PAL fibril from DLS study.

System	Hydrodynamic Radii (nm)	Polydispersity Index (PDI)
Native HEWL fibril	863.06	0.86
HEWL+ PAL (50 μM)fibril	745.77	0.75
HEWL+ PAL (100 μM) fibril	623.66	0.74
HEWL+ PAL (150 μM) fibril	538.69	0.82
HEWL+ PAL (200 μM) fibril	478.35	0.72
HEWL+ PAL (250 μM) fibril	244.12	0.50

without PAL thereby confirming that PAL can resist HEWL fibril formation.

3.2.9. CD

Far UV-CD is a widely used spectroscopic technique to analyze the secondary structural changes in protein. In case of HEWL fibrillation the conformational change of HEWL can also be monitored using this technique. During fibrillation of HEWL α-helix and some unordered structural part is changed into β-sheet conformation. Native HEWL is characterized by negative peak at 208 nm and also with a negative shoulder at 222 nm (α helix 32.80 %, β-sheet 12.80 % and turns and unordered 54.40 %) (Fig. 11B). After 8 h incubation period fibrillar HEWL shows well-defined minima at 222 nm which indicates increase of β-sheet conformations in the protein structure (β-sheet 53.20 %) [57,121]. In presence of PAL the increment in β–sheet content of HEWL is relatively less (β-sheet 45.10 %). As α to β transition with concomitant increase in β sheet content indicate the formation of amyloid fibrillar structures therefore we can conclude that PAL inhibits fibrillation.

3.2.10. AFM

Atomic force microscopy is the most reliable microscopic technique for the 3D morphological characterization of any nano range substance. Both 2D and 3D topographic images of HEWL fibril in absence and presence of PAL are given in Fig. 12. Native HEWL fibril has relatively long network type mature fibrillar structure with higher average height. In presence of PAL HEWL fibrils are less dense and shorter. Average height of these fibrils is certainly low. PAL thus inhibits mature fibril formation and also breaks down the HEWL fibrils.

Interaction of PAL with HEWL has been reported with Na-phosphate buffer (10 mM Na^+) at pH 7.2 [57]. Here this interaction is studied under amyloidogenic condition i.e. Gly-HCl buffer (100 mM Na^+) at pH 2.24. Binding of PAL with HEWL is static in nature with binding constant $(3.98 \pm 0.19) \times 10^4$ M^{-1} at 298 K. Synchronous and 3D fluorescence study reveals tentative conformational change of HEWL. This moderate binding is supported by theoretical studies. In silico docking analysis confirmed that HEWL-PAL complex is stabilized by both hydrogen bonding and hydrophobic interaction. Molecular dynamics simulation

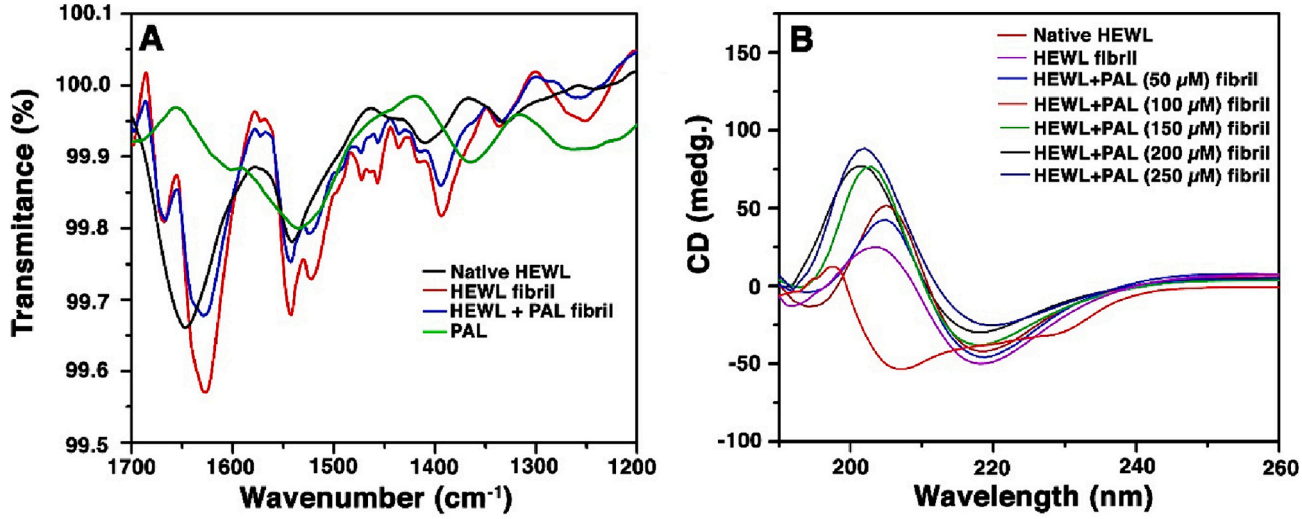

Fig. 11. (A) IR spectrum before and after fibrillation (B) Far-UV CD spectral changes of HEWL during fibrillation.

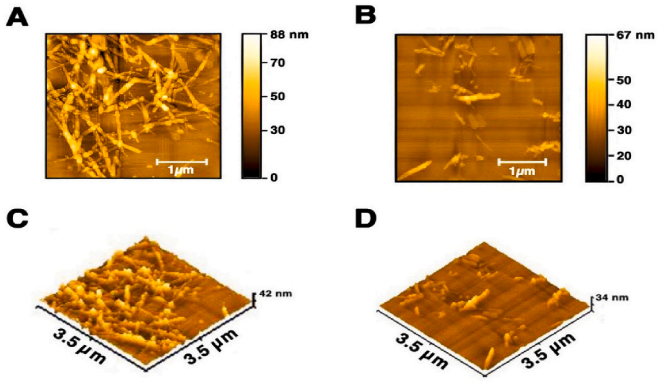

Fig. 12. AFM images of HEWL in the absence (A & C) and presence of PAL (B & D).

result agrees with experimental analysis which clearly confirms that HEWL-PAL complex is stable. The present study reveals that apparent binding constant is slightly decreased with respect to previous study [57].

Modern research work aims to build in depth knowledge about the role of aggregation or deposition of abnormally folded protein in life threatening neurodegenerative disorders. So, the inhibition of protein fibrillation has emerged as a pivotal area of modern research in combating neurodegenerative diseases. Phenolic compounds, indole derivatives, alkaloids, food dyes, thiol based compounds, ionic liquids etc. have been already projected as potential anti-fibrillar compounds [37–43,46,47,52–56]. PAL has been chosen as a potential amyloid inhibitor due to its traditional medicinal uses. Phenolic compounds such as kempferol [122], silybin [123], gallic acid [124], curcuminoid compound [125], resveratrol [126], rosmarinic acid [126] and catechol [50] have shown substantial potential as fibrillation inhibitors. Epigallocatechingallate (400 μM) [127], catechol (100 μg/ml) [50] and curcumin (100 μM) [128] suppresses fibrillation by 70 %, 69 % and 88 %, respectively. Natural alkaloid sanguinarine (50 μM) [56] and coralyne (100 μM) [40] successfully inhibits HEWL fibrillation by 64 % and 97 %, respectively. Different dyes like carmoisine [43], amaranth [42], tartrazine [42], methylene blue [129] have been reported to inhibit fibrillation and dipeptide like carnosine [83] showed more than 60 % inhibition towards HEWL fibrillation at significantly higher working concentration. Our study proves that PAL (250 μM) can securely arrest more than 85 % growth of stable β rich HEWL fibrils which suggest it can act as a highly efficient amyloid inhibitor. A schematic diagram depicting the process of amyloid fibrillation and subsequent inhibition of fibrillation through complexation by PAL is shown in Fig. 13.

4. Conclusions

The current research examines the interaction and inhibitory potential of the isoquinoline alkaloid PAL on protein fibril formation in vitro employing multiple spectroscopic techniques, molecular docking, MD simulation and AFM analysis. PAL significantly quenches the intrinsic fluorescence of HEWL under amyloidogenic conditions and the quenching is static in nature. The binding affinity is moderate and the binding causes microenvironmental changes at the interacting site. Molecular docking analysis complements the spectroscopic data. PAL has a concentration-dependent inhibitory action against HEWL fibrillogenesis. PAL exerts its inhibitory effect by complexation to a partially exposed and aggregation-prone section of HEWL. ANS assay, NR assay and intrinsic fluorescence studies reveal that the changes in surface hydrophobicity, tertiary structure and microenvironment of the amino acid residues in HEWL associated with amyloid fibrillation are effectively suppressed by PAL. CD reveals that PAL can arrest α to β transition in HEWL which is the characteristic of amyloid fibrillation. DLS and

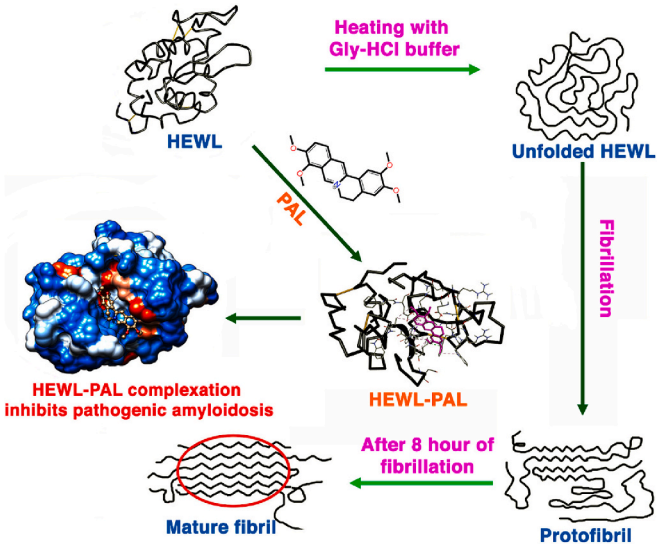

Fig. 13. Schematic diagram depicting HEWL fibrillation and its inhibition through complex formation by PAL.

AFM analysis also testifies unequivocally that PAL can effectively inhibit fibrillation in HEWL. The results from this study yield useful information on antifibrillation properties of alkaloids and can act as model system for development of future drugs in this field.

CRediT authorship contribution statement

Arindam Das: Writing – original draft, Investigation, Formal analysis. **Gouranga Jana:** Writing – original draft, Formal analysis. **Shukdeb Sing:** Writing – original draft, Formal analysis. **Anirban Basu:** Writing – original draft, Funding acquisition, Formal analysis, Conceptualization.

Declaration of competing interest

The authors declare no competing financial interests exist.

Acknowledgements

AB & GJ acknowledge the financial support from the Department of Science and Technology and Biotechnology, Govt. of West Bengal, India (GO No.: 32(Sanc.)-ST/P/S&T/15G-13/2018 dated 31.01.2019). AB acknowledges the assistance provided from DST, Govt. of India, through the FIST grant (Sanction letter No. SR/FST/CS-I/2017/7(C) dated December 28, 2018). SS is a recipient of Junior Research Fellowship from UGC, Govt. of India.

Appendix A. Supplementary data

Supplementary data to this article can be found online at https://doi.org/10.1016/j.ijbiomac.2024.131703.

References

[1] C.M. Dobson, Principles of protein folding, misfolding and aggregation, Semin. Cell Dev. Biol. 15 (2004) 3–16.
[2] S.T. Ferreira, F.G.D. De Felice, A. Chapeaurouge, Metastable, partially folded states in the productive folding and in the misfolding and amyloid aggregation of proteins, Cell Biochem. Biophys. 44 (2006) 539–548.
[3] R.A. Kyle, M.A. Gertz, Systemic amyloidosis, Crit. Rev. Oncol. Hematol. 10 (1990) 49–87.
[4] S. Amani, A. Naeem, Detection and analysis of amorphous aggregates and fibrils of cytochrome c in the presence of phenolic acids, Int. J. Biol. Macromol. 58 (2013) 104–112.

[5] B.H. Toyama, J.S. Weissman, Amyloid structure: conformational diversity and consequences, Annu. Rev. Biochem. 80 (2011) 557–585.
[6] R.N. Rambaran, L.C. Serpell, Amyloid fibrils: abnormal protein assembly, Prion 2 (2008) 112–117.
[7] J. Hardy, D.J. Selkoe, The amyloid hypothesis of Alzheimer's disease: progress and problems on the road to therapeutics, Science 297 (2002) 353–356.
[8] D.B. Kell, Towards a unifying, systems biology understanding of large scale cellular death and destruction caused by poorly liganded iron: Parkinson's, Huntington's, Alzheimer's, prions, bactericides, chemical toxicology and others as examples, Arch. Toxicol. 84 (2010) 825–889.
[9] F. Chiti, C.M. Dobson, Protein misfolding, functional amyloid, and human disease, Annu. Rev. Biochem. 75 (2006) 333–366.
[10] S.S.S. Wang, T.A. Good, An overview of Alzheimer's disease, J. Chin. Inst. Chem. Eng. 36 (2005) 533–559.
[11] D. Eisenberg, M. Jucker, The amyloid state of proteins in human diseases, Cell 148 (2012) 1188–1203.
[12] D.J. Selkoe, Folding proteins in fatal ways, Nature 426 (2003) 900–904.
[13] C.M. Dobson, The structural basis of protein folding and its links with human disease, Philos. Trans. R. Soc. Lond. Ser. B Biol. Sci. 356 (2001) 133–145.
[14] N. Nawaz, S. Wen, F. Wang, S. Nawaz, J. Raza, M. Iftikhar, M. Usman, Lysozyme and its application as antibacterial agent in food industry, Molecules 27 (2022) 6305.
[15] M.A. Mir, Lysozyme: a brief review, Postgrad. Med. J. 53 (1977) 257–259.
[16] C. Pleyer, J. Flesche, F. Saeed, Lysozyme amyloidosis – a case report and review of the literature, Clin. Nephrol. Case Stud. 3 (2015) 42–45.
[17] M. Iqbal, P. Jani, S. Ahmed, T. Sher, First report of hereditary lysozyme amyloidosis in a south Asian family, Case Rep. Hematol. 2019 (2019) 5092496.
[18] L.A. Morozova-Roche, J. Zurdo, A. Spencer, W. Noppe, V. Receveur, D.B. Archer, M. Joniau, C.M. Dobson, Amyloid fibril formation and seeding by wild-type human lysozyme and its disease-related mutational variants, J. Struct. Biol. 130 (2000) 339–351.
[19] M.R.H. Krebs, D.K. Wilkins, E.W. Chung, M.C. Pitkeathly, A.K. Chamberlain, J. Zurdo, C.V. Robinson, C.M. Dobson, Formation and seeding of amyloid fibrils from wild-type hen lysozyme and a peptide fragment from the beta-domain, J. Mol. Biol. 300 (2000) 541–549.
[20] S. Goda, K. Takano, Y. Yamagata, R. Nagata, H. Akutsu, S. Maki, K. Namba, K. Yutani, Amyloid protofilament formation of hen egg lysozyme in highly concentrated ethanol solution, Protein Sci. 9 (2000) 369–375.
[21] L.N. Arnaudov, R. de Vries, Thermally induced fibrillar aggregation of hen egg white lysozyme, Biophys. J. 88 (2005) 515–526.
[22] F. Meersman, K. Heremans, Temperature-induced dissociation of protein aggregates: accessing the denatured state, Biochemistry 42 (2003) 14234–14241.
[23] E. Frare, M.F. Mossuto, P.P. de Laureto, S. Tolin, L. Menzer, M. Dumoulin, C. M. Dobson, A. Fontana, Characterization of oligomeric species on the aggregation pathway of human lysozyme, J. Mol. Biol. 387 (2009) 17–27.
[24] E. Frare, P.P.D. Laureto, J. Zurdo, C.M. Dobson, A. Fontana, A highly amyloidogenic region of hen lysozyme, J. Mol. Biol. 340 (2004) 1153–1165.
[25] G. Merlini, V. Bellotti, Lysozyme: a paradigmatic molecule for the investigation of protein structure, function and misfolding, Clin. Chim. Acta 357 (2005) 168–172.
[26] Z. Gu, X. Zhu, S. Ni, Z. Su, H.M. Zhou, Conformational changes of lysozyme refolding intermediates and implications for aggregation and renaturation, Int. J. Biochem. Cell Biol. 36 (2004) 795–805.
[27] L.J. Smith, M.J. Sutcliffe, C. Redfield, C.M. Dobson, Structure of hen lysozyme in solution, J. Mol. Biol. 229 (1993) 930–944.
[28] A. Ghosh, K.V. Brinda, S. Vishveahwara, Dynamics of lysozyme structure network: probing the process of unfolding, Biophys. J. 92 (2007) 2523–2535.
[29] T. Imoto, L.S. Forster, J.A. Rupley, F. Tanaka, Fluorescence of lysozyme: emissions from tryptophan residues 62 and 108 and energy migration, Proc. Natl. Acad. Sci. USA 69 (1972) 1151–1155.
[30] J. Held, S.V. van Smaalen, The active site of hen egg-white lysozyme: flexibility and chemical bonding, Acta Crystallogr. D Biol. Crystallogr. 70 (2014) 1136–1146.
[31] C. Jash, P.V. Payghan, N. Ghoshal, G.S. Kumar, Binding of the iminium and alkanolamine forms of sanguinarine to lysozyme: spectroscopic analysis, thermodynamics, and molecular modeling studies, J. Phys. Chem. B 118 (2014) 13077–13091.
[32] N.C.J. Strynadka, M.N.G. James, Lysozyme revisited crystallographic evidence for distortion of an N-acetylmuramic acid residue bound in site D, J. Mol. Biol. 220 (1991) 401–424.
[33] Z.R. Zhang, Q. Zheng, J. Han, G.P. Gao, J. Liu, T. Gong, Z. Gu, Y. Huang, X. Sun, Q. He, The targeting of 14-succinate triptolide-lysozyme conjugate to proximal renal tubular epithelial cells, Biomaterials 30 (2009) 1372–1381.
[34] S. Fujiwara, F. Matsumoto, Y. Yonezawa, Effects of salt concentration on association of the amyloid protofilaments of hen egg white lysozyme studied by time-resolved neutron scattering, J. Mol. Biol. 331 (2003) 21–28.
[35] S. Raccosta, V. Martorana, M. Manno, Thermodynamic versus conformational metastability in fibril forming lysozyme solutions, J. Phys. Chem. B 116 (2012) 12078–12087.
[36] A. Sgarbossa, Natural biomolecules and protein aggregation: emerging strategies against amyloidogenesis, Int. J. Mol. Sci. 13 (2012) 17121–17137.
[37] N. Ferreira, M.J. Saraiva, M.R. Almeida, Natural polyphenols inhibit different steps of the process of transthyretin (TTR) amyloid fibril formation, FEBS Lett. 585 (2011) 2424–2430.
[38] S.C. How, S.M. Yang, A. Hsin, C.P. Tseng, S.S. Hsueh, M.S. Lin, R.P.Y. Chen, W. L. Chou, S.S.S. Wang, Examining the inhibitory potency of food additive fast green FCF against amyloid fibrillogenesis under acidic conditions, Food Funct. 7 (2016) 4898–4907.
[39] I. Hafner-Bratkovic, J. Gaspersic, L.M. Smid, M. Bresjanac, R. Jerala, J. Neurochem, Curcumin binds to the -helical intermediate and to the amyloid form of prion protein – a new mechanism for the inhibition of PrP (Sc) accumulation, J. Neurochem. 104 (2008) 1553–1564.
[40] A. Basu, A. Mahammad, A. Das, Inhibition of the formation of lysozyme fibrillar assemblies by the isoquinoline alkaloid coralyne, New J. Chem. 46 (2022) 3258–3269.
[41] D. Mishra, D. Sellin, A. Radovan, R. Gohlke, Winter, inhibiting islet amyloid polypeptide fibril formation by the red wine compound resveratrol, chem, Biol. Chem. 10 (2009) 445–449.
[42] A. Basu, G.S. Kumar, Binding and inhibitory effect of dyes amaranth and tartrazine on amyloid fibrillation in lysozyme, J. Phys. Chem. B 121 (2017) 1222–1239.
[43] A. Basu, G.S. Kumar, Interaction and inhibitory influence of the azo dye carmoisine on lysozyme amyloid fibrillogenesis, Mol. BioSyst. 13 (2017) 1552–1564.
[44] G. Gao, M. Zhang, D. Gong, R. Chen, X. Hu, T. Sun, The size-effect of gold nanoparticles and nanoclusters in the inhibition of amyloid-β fibrillation, Nanoscale 9 (2017) 4107–4113.
[45] S. Xiao, D. Zhou, P. Luan, B. Gu, L. Feng, S. Fan, W. Liao, W. Fang, L. Yang, E. Tao, R. Guo, J. Liu, Graphene quantum dots conjugated neuroprotective peptide improve learning and memory capability, Biomaterials 106 (2016) 98–110.
[46] H.R. Kalhor, M. Kamizi, J. Akbari, A. Heydari, Inhibition of amyloid formation by ionic liquids: ionic liquids affecting intermediate oligomers, Biomacromolecules 10 (2009) 2468–2475.
[47] S.S.S. Wang, K.N. Liu, B.W. Wang, Effects of dithiothreitol on the amyloid fibrillogenesis of hen egg-white lysozyme, Eur. Biophys. J. 39 (2010) 1229–1242.
[48] Q.I. Churches, J. Caine, K. Cavanagh, V.C. Epa, L. Waddington, C.E. Tranberg, A. G. Meyer, J.N. Varghese, V. Streltsov, P.J. Duggan, Naturally occurring polyphenolic inhibitors of amyloid beta aggregation, Bioorg. Med. Chem. Lett. 24 (2014) 3108–3112.
[49] S. Sen, S. Konar, B. Das, A. Pathak, S. Dhara, S. Dasgupta, S. DasGupta, Inhibition of fibrillation of human serum albumin through interaction with chitosan-based biocompatible silver nanoparticles, RSC Adv. 6 (2016) 43104–43115.
[50] S. Feng, X.H. Song, C.M. Zeng, Inhibition of amyloid fibrillation of lysozyme by phenolic compounds involves quinoprotein formation, FEBS Lett. 586 (2012) 3951–3955.
[51] K. Ono, M. Yamada, Antioxidant compounds have potent anti-fibrillogenic and fibril-destabilizing effects for α-synuclein fibrils in vitro, J. Neurochem. 97 (2006) 105–115.
[52] P. Velander, L. Wu, F. Henderson, S. Zhang, D.R. Bevan, B. Xu, Natural product-based amyloid inhibitors, Biochem. Pharmacol. 139 (2017) 40–55.
[53] 53. G. Hussain, A. Rasul, H. Anwar, N. Aziz, A. Razzaq, W. Wei, M. Ali, J. Li, X. Li, Role of plant derived alkaloids and their mechanism in neurodegenerative disorders, Int. J. Biol. Sci. 14 (2018) 341–357.
[54] A.Y. Khan, G.S. Kumar, Natural isoquinoline alkaloids: binding aspects to functional proteins, serum albumins, hemoglobin, and lysozyme, Biophys. Rev. 7 (2015) 407–420.
[55] C. Jash, P. Basu, P.V. Payghan, N. Ghoshal, G.S. Kumar, Chelerythrine–lysozyme interaction: spectroscopic studies, thermodynamics and molecular modeling exploration, Phys. Chem. Chem. Phys. 17 (2015) 16630–16645.
[56] A. Basu, S. Sing, A. Das, G. Jana, B. Samai, Interaction and inhibition of lysozyme amyloid fibrillation by benzophenanthridine alkaloid sanguinarine: photophysical, molecular docking and imaging studies, J. Photochem. Photobiol. A 444 (2023) 114996.
[57] C. Jash, G.S. Kumar, Binding of alkaloids berberine, palmatine and coralyne to lysozyme: a combined structural and thermodynamic study, RSC Adv. 4 (2014) 12514–12525.
[58] H. Ashrafian, E.H. Zadeh, M. Tajbakhsh, N. Majid, G.N. Srivastava, R.H. Khan, Discovery of a tetracyclic indole alkaloid that postpones fibrillation of hen egg white lysozyme protein, Int. J. Biol. Macromol. 183 (2021) 1939–1947.
[59] J. Long, J. Song, L. Zhong, Y. Liao, L. Liu, X. Li, Palmatine: a review of its pharmacology, toxicity and pharmacokinetics, Biochimie 162 (2019) 176–184.
[60] B. Ma, L. Zhu, X. Zang, Y. Chen, D. Li, Y. Wang, Coptischinensis inflorescence and its main alkaloids protect against ultraviolet-B-induced oxidative damage, J. Funct. Foods 5 (2013) 1665–1672.
[61] Y. Deng, M. Zhang, H. Luo, Identification and antimicrobial activity of two alkaloids from traditional Chinese medicinal plant *Tinosporacapillipes*, Ind. Crop. Prod. 37 (2012) 298–302.
[62] Z.C. Li, X.B. Kong, W.P. Mai, G.C. Sun, S.Z. Zhao, Synthesis and antimicrobial activity of 9-O-substituted palmatine derivatives, Indian J. Pharm. Sci. 77 (2015) 196–201.
[63] G. Chen, Y. Xu, J. Jing, B. Mackie, X. Zheng, X. Zhang, J. Wang, X. Li, The anti-sepsis activity of the components of Huanglian Jiedu decoction with high lipid A-binding affinity, Int. Immunopharmacol. 46 (2017) 87–96.
[64] D. Kaufmann, A. K. Dogra, A. Tahrani, F. Herrmann. M. Wink, Extracts from traditional Chinese medicinal plants inhibit acetylcholinesterase, a known Alzheimer's disease target, Molecules 21(2016) 1161.
[65] L. Zhang, J. Li, F. Ma, S. Yao, N. Li, J. Wang, Y. Wang, X. Wang, Q. Yao, Synthesis and cytotoxicity evaluation of 13-n-alkyl berberine and palmatine analogues as anticancer agents, Molecules 17 (2012) 11294–11302.
[66] M.B. Patel, S. Mishra, Hypoglycemic activity of alkaloidal fraction of Tinosporacordifolia, Phytomedicine 18 (2011) 1045–1052.

[67] D.R. Booth, M. Sunde, V. Bellotti, C.V. Robinson, W.L. Hutchinson, P.E. Fraser, P. N. Hawkins, C.M. Dobson, S.E. Radford, C.C.F. Blake, M.B. Pepys, Instability, unfolding and aggregation of human lysozyme variants underlying amyloid fibrillogenesis, Nature 385 (1997) 787–793.
[68] R.F. Steiner, L. Weinry, Excited States of Protein and Nucleic Acid, Plenum Press, 1971.
[69] J.N. Miller, Recent developments in fluorescence and chemiluminescence analysis, Plenary lecture, Analyst 109 (1984) 191–198.
[70] J.R. Lakowicz, Principles of Fluorescence Spectroscopy, 2009.
[71] N. Shahabadi, M. Maghsudi, Z. Kiani, M. Pourfoulad, Multispectroscopic studies on the interaction of 2-tert-butylhydroquinone (TBHQ), a food additive, with bovine serum albumin, Food Chem. 124 (2011) 1063–1068.
[72] L. Stryer, R.P. Haugland, Energy transfer: a spectroscopic ruler, Proc. Natl. Acad. Sci. USA 58 (1967) 719–726.
[73] S.F. Sousa, P.A. Fernandes, M.J. Ramos, Protein-ligand docking: current status and future challenges, Proteins 65 (2006) 15–26.
[74] E. De la Mora, I. Carmichael, E.F. Garman, Effective scavenging at cryotemperatures: further increasing the dose tolerance of protein crystals, J. Synchrotron Radiat. 18 (2011) 346–357.
[75] G. Paramaguru, A. Kathiravan, S. Selvaraj, P. Venuvanalingam, R. Renganathan, Interaction of anthraquinone dyes with lysozyme: evidences from spectroscopic and docking studies, J. Hazard. Mater. 175 (2010) 985–991.
[76] G.M. Morris, D.S. Goodsell, R.S. Halliday, R. Huey, W.E. Hart, R.K. Belew, A. J. Olson, Automated docking using a Lamarckian genetic algorithm and an empirical binding free energy function, J. Comput. Chem. 19 (1998) 1639–1662.
[77] S.K. Atkovska, A. Samsonov, M.P. Rogacz, M.T. Pisabarro, Multiple ligand simultaneous docking (MLSD): a novel approach to study the effect of inhibitors on substrate binding to PPO, Int. J. Mol. Sci. 15 (2014) 2622–2645.
[78] E. Lindahl, B. Hess, D. van der Spoel, GROMACS, 3.0: a package for molecular simulation and trajectory analysis, J. Mol. Model. 7 (2001) 306–317.
[79] A. Kroes-Nijboer, P. Venema, J. Bouman, E. van der Linden, Influence of protein hydrolysis on the growth kinetics of β-lg fibrils, Langmuir 27 (2011) 5753–5761.
[80] L. Nielsen, R. Khurana, A. Coats, S. Frokjaer, J. Brange, S. Vyas, V.N. Uversky, A. L. Fink, Effect of environmental factors on the kinetics of insulin fibril formation: elucidation of the molecular mechanism, Biochemistry 40 (2001) 6036–6046.
[81] N. Darghal, A. Garnier-Suillerot, M. Salerno, Mechanism of Thioflavin T accumulation inside cells overexpressing P-glycoprotein or multidrug resistance-associated protein: role of lipophilicity and positive charge, Biochem. Biophys. Res. Commun. 343 (2006) 623–629.
[82] G. Weber, L.B. Young, Fragmentation of bovine serum albumin by pepsin. I. The origin of the acid expansion of the albumin molecule, J. Biol. Chem. 239 (1964) 1415–1423.
[83] J.W. Wu, K.N. Liu, S.C. How, W.A. Chen, C.M. Lai, H.S. Liu, C.J. Hu, S.S.-S. Wang, Carnosine's effect on amyloid fibril formation and induced cytotoxicity of lysozyme, PLoS One 8 (2013) e81982.
[84] C.M. Pfefferkorn, R.P. McGlinchey, J.C. Lee, Effects of pH on aggregation kinetics of the repeat domain of a functional amyloid, Pmel17, Proc. Natl. Acad. Sci. USA 107 (2010) 21447–21452.
[85] S.W. Provencher, J. Glöckner, Estimation of globular protein secondary structure from circular dichroism, Biochemistry 20 (1981) 33–37.
[86] I.H.M. Van Stokkum, H.J.W. Spoelder, M. Bloemendal, R. Van Grondelle, F.C. A. Groen, Estimation of protein secondary structure and error analysis from circular dichroism spectra, Anal. Biochem. 191 (1990) 110–118.
[87] N. Sreerama, R.W. Woody, Estimation of protein secondary structure from circular dichroism spectra: comparison of CONTIN, SELCON, and CDSSTR methods with an expanded reference set, Anal. Biochem. 287 (2000) 252–260.
[88] L. Whitmore, B.A. Wallace, DICHROWEB, an online server for protein secondary structure analyses from circular dichroism spectroscopic data, Nucleic Acids Res. 32 (2004) W668–W673.
[89] L. Whitmore, B.A. Wallace, Protein secondary structure analyses from circular dichroism spectroscopy: methods and reference databases, Biopolymers 89 (2008) 392–400.
[90] A. Basu, G.S. Kumar, Interaction of toxic azo dyes with heme protein: biophysical insights into the binding aspect of the food additive amaranth with human haemoglobin, J. Hazard. Mater. 289 (2015) 204–209.
[91] A. Basu, G.S. Kumar, Binding of carmoisine, a food colorant, with hemoglobin: spectroscopic and calorimetric studies, Food Res. Int. 72 (2015) 54–61.
[92] E. Nishimoto, S. Yamashita, N. Yamasaki, T. Imoto, Resolution and characterization of tryptophyl fluorescence of hen egg-white lysozyme by quenching and time-resolved spectroscopy, Biosci. Biotechnol. Biochem. 63 (1999) 329–336.
[93] K. Hayashi, T. Imoto, G. Funatsu, M. Funatsu, The position of the active tryptophan residue in lysozyme, J. Biochem. 58 (1965) 227–235.
[94] A.P. Demchenko, Ultraviolet spectroscopy of protein, Springer-Verlag 198 (1986) 312.
[95] Z. Chi, S.A. Asher, UV Raman determination of the environment and solvent exposure of Tyr and Trp residues, J. Phys. Chem. B 102 (1998) 9595–9602.
[96] J.B.F. Lloyd, Synchronized excitation of fluorescence emission spectra, Nat. Phys. Sci. 231 (1971) 64–65.
[97] F.C. Wu, R.B. Mills, R.D. Evans, P.J. Dillon, Kinetics of metal-fulvic acid complexation using a stopped-flow technique and three-dimensional excitation emission fluorescence spectrophotometer, Anal. Chem. 76 (2004) 110–113.
[98] F. Ding, W. Liu, Y. Li, L. Zhang, Y. Sun, Determining the binding affinity and binding site of bensulfuron-methyl to human serum albumin by quenching of the intrinsic tryptophan fluorescence, JOL 130 (2010) 2013–2021.
[99] J.R. Lakowicz, Principles of Fluorescence Spectroscopy, third edition, Springer Science, 2006.
[100] W. Peng, F. Ding, Y.K. Peng, Y.T. Jiang, L. Zhang, Binding patterns and structure-affinity relationships of food azo dyes with lysozyme: a multitechnique approach, J. Agric. Food Chem. 61 (2013) 12415–12428.
[101] O.K. Abou-Zied, O.I.K. Al-Shihi, Characterization of subdomain IIA binding site of human serum albumin in its native, unfolded, and refolded states using small molecular probes, J. Am. Chem. Soc. 130 (2008) 10793–10801.
[102] C.A. Lipinski, F. Lombardo, B.W. Dominy, P.J. Feeney, Experimental and computational approaches to estimate solubility and permeability in drug discovery and development settings, Adv. Drug Deliv. Rev. 23 (2008) 3–25.
[103] P.S. Vassar, C.F.A. Culling, Fluorescent stains, with special reference to amyloid and connective tissues, Arch. Pathol. 68 (1959) 487–498.
[104] A. Basu, Examining the effect of the crown ether, 18-crown-6, on lysozyme fibrillation, New J. Chem. 47 (2023) 2924–2931.
[105] W.G. Turnell, J.T. Finch, Binding of the dye congo red to the amyloid protein pig insulin reveals a novel homology amongst amyloid-formin peptide sequences, J. Mol. Biol. 227 (1992) 1205–1223.
[106] W.E. Klunk, R.F. Jacob, R.P. Mason, Quantifying amyloid by Congo red spectral shift assay, Methods Enzymol. 309 (1999) 285–305.
[107] P. Ladewig, Double-refringence of the amyloid-Congo-red-complex in histological sections, Nature 156 (1945) 81–82.
[108] B. Bolognesi, J.R. Kumita, T.P. Barros, E.K. Esbjorner, L.M. Luheshi, D. C. Crowther, M.R. Wilson, C.M. Dobson, G. Favrin, J.J. Yerbury, ANS binding reveals common features of cytotoxic amyloid species, ACS Chem. Biol. 5 (2010) 735–740.
[109] S.K. Chaturvedi, P. Alam, J.M. Khan, M.K. Siddiqui, P. Kalaiarasan, N. Subbarao, Z. Ahmad, R.H. Khan, Biophysical insight into the anti-amyloidogenicbehavior of taurine, Int. J. Biol. Macromol. 80 (2015) 375–384.
[110] P.J.G. Coutinho, Photophysics and biophysical applications of benzo[a] phenoxazine type fluorophores, Rev. Fluoresc. (2009) 335–362.
[111] C. Formoso, L.S. Forster, Tryptophan fluorescence lifetimes in lysozyme, J. Biol. Chem. 250 (1975) 3738–3745.
[112] M. Rholam, S. Scarlata, G. Weber, Frictional resistance to the local rotations of fluorophores in proteins, Biochemistry 23 (1984) 6793–6796.
[113] M.R. Eftink, Fluorescence techniques for studying protein-structure, Methods Biochem. Anal. 35 (1991) 127–205.
[114] Y. Chen, M.D. Barkley, Toward understanding tryptophan fluorescence in proteins, Biochemistry 37 (1998) 9976–9982.
[115] J.T. Vivian, P.R. Callis, Mechanisms of tryptophan fluorescence shifts in proteins, Biophys. J. 80 (2001) 2093–2109.
[116] A. Chaari, C. Fahy, A. Chevillot-Biraud, M. Rholam, Insights into kinetics of agitation-induced aggregation of hen lysozyme under heat and acidic conditions from various spectroscopic methods, PLoS One 10 (2015) e0142095.
[117] S. Bhattacharya, N.K. Pandey, A. Roy, S. Dasgupta, Effect of (−)-epigallocatechingallate on the fibrillation of human serum albumin, Int. J. Biol. Macromol. 70 (2014) 312–319.
[118] J.M. Khan, S.K. Chaturvedi, S.K. Rahman, M. Ishtikhar, A. Qadeer, E. Ahmad, R. H. Khan, Protonation favors aggregation of lysozyme with SDS, Soft Matter 10 (2014) 2591–2599.
[119] A. Giugliarelli, L. Tarpani, L. Latterini, A. Morresi, M. Paolantoni, P. Sassi, Spectroscopic and microscopic studies of aggregation and fibrillation of lysozyme in water/ethanol solutions, J. Phys. Chem. B 119 (2015) 13009–13017.
[120] Z. Islam, M.H. Ali, A. Popelka, R. Mall, E. Ullah, J. Ponraj, P.R. Kolatkar, Probing the fibrillation of lysozyme by nanoscale-infrared spectroscopy, J. Biomol. Struct. Dyn. 39 (2021) 1481–1490.
[121] A. Basu, S.C. Bhattacharya, G.S. Kumar, Influence of the ionic liquid 1-butyl-3-methylimidazolium bromide on amyloid fibrillogenesis in lysozyme: evidence from photophysical and imaging studies, Int. J. Biol. Macromol. 107 (2018) 2643–2649.
[122] M.S. Borana, P. Mishra, R.R.S. Pissurlenkar, R.V. Hosur, B. Ahmad, Curcumin and kaempferol prevent lysozyme fibril formation by modulating aggregation kinetic parameters, Biochim. Biophys. Acta 2014 (1844) 670–680.
[123] X. Chen, X. Deng, X. Han, Y. Liang, Z. Meng, R. Liu, W. Su, H. Zhu, T. Fu, Inhibition of lysozyme amyloid fibrillation by silybin diastereoisomers: the effects of stereochemistry, ACS Omega 6 (2021) 3307–3318.
[124] M. Konar, S. Bag, P. Roy, S. Dasgupta, Gallic acid induced dose dependent inhibition of lysozyme fibrillation, Int. J. Biol. Macromol. 103 (2017) 1224–1231.
[125] F. Mohammadi, A. Mahmudian, M. Moeeni, L. Hassani, Inhibition of amyloid fibrillation of hen egg-white lysozyme by the natural and synthetic curcuminoids, RSC Adv. 6 (2016) 23148–23160.
[126] S. Shariatizi, A.A. Meratan, A. Ghasemi, M. Nemat-Gorgani, Inhibition of amyloid fibrillation and cytotoxicity of lysozyme fibrillation products by polyphenols, Int. J. Biol. Macromol. 80 (2015) 95–106.
[127] F.K. Zaidi, R. Bhat, Two polyphenols with diverse mechanisms towards amyloidosis: differential modulation of the fibrillation pathway of human lysozyme by curcumin and EGCG, J. Biomol. Struct. Dyn. 40 (2022) 4593–4611.
[128] S.S. Wang, K.N. Liu, W.H. Lee, Effect of curcumin on the amyloid fibrillogenesis of hen egg-white lysozyme, Biophys. Chem. 144 (2009) 78–87.
[129] S.C. How, Y.H. Cheng, C.H. Lo, J.T. Lai, T.H. Lin, Z. Bednarikova, A. Antosova, Z. Gazova, J.W. Wu, S.S.-S. Wang, Exploring the effects of methylene blue on amyloid fibrillogenesis of lysozyme, Int. J. Biol. Macromol. 119 (2018) 1059–1067.